Editors' Suggestion

Effects of finite spatial and temporal resolution in direct numerical simulations of incompressible isotropic turbulence

P. K. Yeung*
Schools of Aerospace Engineering and Mechanical Engineering, Georgia Institute of Technology, Atlanta, Georgia 30332, USA

K. R. Sreenivasan
Department of Mechanical and Aerospace Engineering, Department of Physics, and Courant Institute of Mathematical Sciences, New York University, New York, New York 10012, USA

S. B. Pope
Sibley School of Mechanical and Aerospace Engineering, Cornell University, Ithaca, New York 14853, USA

(Received 26 February 2018; published 18 June 2018)

As computing power has grown and turbulent flows at increasing Reynolds numbers are being computed by direct numerical simulations, conventional assumptions on adequate spatial and temporal resolutions are being continually challenged. We perform a systematic study of the resolution effects via numerical simulations at various spatial and temporal resolutions to clarify the proper scaling of dissipation and enstrophy (vorticity squared). Results show that inadequate resolution in space and/or time leads to overestimation of the likelihood and intensity of extreme fluctuations in dissipation and enstrophy. In order to capture rare events accurately, for instance, one needs to have not only grid resolutions that are increasingly smaller fractions of the Kolmogorov scale as the Reynolds number increases but also the Courant number that becomes increasingly smaller than that assumed to be adequate previously. Some comparisons are made with results obtained from an alternative approach where a stricter criterion for truncation in wave-number space allows aliasing errors to be removed completely. In contrast to prior work, the present data do not support the notion that dissipation and enstrophy probability density functions (PDFs) approach each other in the far tails at high Reynolds number. However the two PDFs are remarkably similar in form, being well described by stretched exponentials.

DOI: 10.1103/PhysRevFluids.3.064603

I. INTRODUCTION

Rapid advances in computing power, especially since the beginning of this century, have continued to enable direct numerical simulations (DNS) of ever-larger magnitude and/or greater physical complexity, including both homogeneous [1,2] and inhomogeneous turbulent flows [3,4], using many billions, or even trillions, of grid points. For homogeneous turbulence, the goals pursued by various authors have included the attainment of as high a Reynolds number as possible to study the asymptotic properties of small scales, the understanding of turbulent mixing at Schmidt numbers as high as possible, and to incorporate more physical processes such as stratification and magnetic fields that typically require a much wider parameter space to be addressed. However, it is understood that no simulation is completely error-free, especially where some more sensitive quantities (such

*pk.yeung@ae.gatech.edu

as higher order moments or the statistics of extreme fluctuations) are concerned. Consequently, it is important to identify and address limitations in current practices in the simulations, and use this knowledge to clarify how the tremendous resources needed at the next level can be best utilized.

In general, accuracy in DNS depends on a combination of truncation (discretization) errors in space and time, aliasing errors arising from nonlinear products while using pseudospectral methods, as well as limitations in statistical sampling. A common approach to obtain higher accuracy is to increase the spatial resolution, while keeping key physical parameters (such as the Reynolds number) unchanged [5,6]. For production simulations that are already pushing the limits of the state-of-the-art computing facilities, further grid refinement is clearly very challenging. At the same time, for a given spatial resolution it is useful to investigate the effects of aliasing errors on small-scale quantities, and of errors from finite temporal resolution (which is connected to spatial resolution when explicit numerical schemes are used for integration in time). In particular, while most discussions [7,8] of resolution requirements have been focused on spatial grid spacing, time-stepping errors may also be very significant when fast-changing events of high amplitude occur, or when the small-scale structure is swept through the solution domain rapidly by the large scales [9].

In this paper we focus on the effects of both spatial and temporal resolutions on events of extreme amplitude in the energy dissipation rate and enstrophy, which are defined respectively as

$$\epsilon = 2\nu s_{ij} s_{ij}, \quad \Omega = \omega_i \omega_i \tag{1}$$

(where ν is the kinematic viscosity, s_{ij} is the strain rate, ω_i is the vorticity). The importance of these quantities in intermittency theories is well established [10]. We take two approaches. First, we take a number of high-resolution datasets, apply a filter that removes high wave numbers beyond a certain cutoff, and observe the effect of this cutoff on various statistics of dissipation and enstrophy fluctuations. These comparisons provide strong evidence that regardless of the spatial resolution, results on extreme fluctuations are strongly associated with high wave-number modes that are not completely free of aliasing errors. Although less intermittent than enstrophy (at least at Reynolds numbers covered so far), dissipation fluctuations are found to be more sensitive to the choice of cutoff wave number in this filtering procedure. Second, to include the effects of time-stepping errors, we compare results on extreme events of dissipation and enstrophy from simulations at different grid resolutions and at different choices of the time step (Δt). Even simulations over short time spans (say, of the order of 10 Kolmogorov timescales) are helpful in this regard, because they allow us to revisit, with some degree of certainty, the issue of whether extreme events in dissipation and enstrophy truly scale in the manner described in [1,11].

The remaining sections of this paper are organized as follows. In Sec. II we first provide a brief summary of the numerical algorithms employed, and of the measures of spatial and temporal resolution applicable to our simulations. Results at different levels of spatial and temporal resolution at multiple Reynolds numbers are presented in Sec. III, ultimately leading to a new interpretation of the likelihood and magnitude of extreme events in dissipation and enstrophy using the best results available at a given Reynolds number. Finally, in Sec. IV, we summarize the findings of this work and briefly discuss their implications for future research.

II. NUMERICAL METHODS, RESOLUTION IN SPACE AND TIME

Although the approaches adopted here are general, we focus on results from direct numerical simulations (DNS) of incompressible isotropic turbulence on a three-dimensional (3D) periodic domain. The simulations are forced by maintaining the energy spectrum $E(k)$ at low wave numbers [12] ($k \leqslant k_F$, where $k_F = 3$) at values based on long-time averages in prior simulations that used stochastic forcing [13]. Provided the forcing scales are sufficiently far removed from those ranges associated with the large dissipation and enstrophy fluctuations, we may expect the details of the forcing to have no significant impact on the issues under discussion. The Reynolds number is varied by changing the viscosity. We use a massively parallel implementation of a well-known Fourier pseudospectral algorithm [14], which uses both phase shifting and truncation in wave-number space

for control of aliasing errors. On an N^3 domain with length 2π units on each side the highest resolvable wave number is $k_{\max} = \sqrt{2}N/3$. In simulations of this type spatial resolution of the small scales is often expressed by the nondimensional parameter $k_{\max}\eta$, where $\eta = (\nu^3/\langle\epsilon\rangle)^{1/4}$ is the Kolmogorov length scale. Here angled brackets represent averaging in space. However, since the turbulence is also statistically stationary, time averaging is also applicable when evaluating statistics such as the value of η used to quantify spatial resolution, and, also later, when results on probability density functions (PDFs) of dissipation and enstrophy are shown. The ratio between the grid spacing and η can be written as

$$\frac{\Delta x}{\eta} = \frac{\sqrt{2}}{3}\frac{2\pi}{k_{\max}\eta} \approx \frac{2.96}{k_{\max}\eta}. \tag{2}$$

For low-order statistics a value of $k_{\max}\eta$ of order 1.5 (without truly resolving the smallest scales) may be adequate. However, because of intermittency, larger values of $k_{\max}\eta$ are required for higher order statistics influenced by the occurrence of dissipation fluctuations much larger than the mean, especially at higher Reynolds number.

For an existing DNS velocity saved from a prior simulation we can readily apply a series of sharp spectral cutoffs in wave-number space,

$$\hat{\mathbf{u}}^i(\mathbf{k}) = \begin{cases} \hat{\mathbf{u}}^0(\mathbf{k}) & \text{if } |\mathbf{k}| \leqslant k_c^i \leqslant k_{\max}, \\ 0 & \text{otherwise,} \end{cases} \tag{3}$$

where it is convenient for cutoff wave number k_c^i to be reduced monotonically from $k_{\max}$ downwards. The filtering operation embodied here can also be interpreted as a reduction of grid resolution from N^3 to $(3k_c^i/\sqrt{2})^3$ grid points. Each truncated velocity field can be used to compute the statistics of quantities such as dissipation and enstrophy, with contributions from velocity modes of wave numbers higher than k_c^i removed. This post-processing calculation requires far less resources than a new simulation at a different grid resolution. If a statistic in question, such as the PDF of the normalized dissipation rate $\epsilon/\langle\epsilon\rangle$ differs strongly between results at two different resolution levels (corresponding to k_c^i and k_c^{i+1}, say) then this result is sensitive to resolution. This sensitivity is likely to be substantial for nonlinear quantities, such as dissipation rate fluctuations, which (by the nature of Fourier transforms of nonlinear products) have spectral content beyond k_c^i. In contrast, the difference should be weak for quantities dominated by the large scales with no intermittency, such as the kinetic energy and the averaged dissipation rate ($\langle\epsilon\rangle$).

When Fourier pseudospectral methods are used the Navier-Stokes equations are transformed to ordinary differential equations in wave-number space, which are advanced in time using explicit Runge-Kutta (RK) schemes for the advective terms, while viscous terms are treated exactly via an integrating factor. We use a second-order (RK2) scheme, with the time step subject to a constraint for numerical stability expressed in terms of the Courant number,

$$C = \Delta t\left[\frac{|u|}{\Delta x} + \frac{|v|}{\Delta y} + \frac{|w|}{\Delta z}\right]_{\max}, \tag{4}$$

where the maximum is taken over all (N^3) grid points. The expression within square brackets in Eq. (4) is a random variable, which (with $\Delta x, \Delta y, \Delta z$ all equal) can be expected to scale with $u'/\Delta x$, by a coefficient, say β, which itself is determined by the (Gaussian) probability distribution of the velocity fluctuations. (In our simulations $\beta \approx 12$, which could correspond to samples where all three velocity components take values 4 times the standard deviation simultaneously.)

It is helpful to recast the time increment Δt in terms of the Kolmogorov timescale τ_η. Using the classical isotropy relation $\langle\epsilon\rangle = 15\nu\langle(\partial u/\partial x)^2\rangle$ then gives

$$\Delta t/\tau_\eta \approx (C/\beta)(15)^{1/4}(\Delta x/\eta){R_\lambda}^{-1/2}, \tag{5}$$

where τ_η is the Kolmogorov timescale, and $R_\lambda = u'\lambda/\nu$ is the Taylor-scale Reynolds number. This shows that (for fixed C) $\Delta t/\tau_\eta$ is proportional to $\Delta x/\eta$ but decreases as ${R_\lambda}^{-1/2}$.

In simulations at high R_λ it is typical for $\Delta t/\tau_\eta$ to be order 1% of less. However, as we shall see later, although (in contrast to $\Delta x/\eta$) $\Delta t/\tau_\eta$ is much smaller than unity, time-stepping errors can still be significant. This suggests, that τ_η is, in fact, not the smallest timescale that needs to be resolved. Instead, two smaller timescales are η/u', which characterizes advective transport of the small scales by the large-scale motions [9], and $\Delta x/u'$, which is a numerical advection timescale determined by the grid spacing. With the relation $C = \beta u' \Delta t/\Delta x$ as well as Eq. (2) we can write

$$\Delta t/(\eta/u') \approx \frac{C}{\beta}\frac{3}{k_{\max}\eta}. \tag{6}$$

This relation suggests a higher $k_{\max}\eta$ may allow the use of a higher Courant number; and that a lower Courant number may have effects somewhat similar to that of a higher $k_{\max}\eta$, which is to be tested in the work presented in this paper.

In addition to the size of the time step, it is clear that the time-stepping error also depends on the details of the time-stepping scheme and the alias-removal technique applied. To facilitate comparisons with prior work [1,11] we have chosen to focus here on results obtained using RK2 integration. Numerical tests using a fourth-order (RK4) scheme do appear to give smaller errors, as expected. However, for the highly nonlinear quantities in this paper, the presence of residual aliasing errors of order $(\Delta t)^2$ in Rogallo's algorithm precludes a clear demonstration of fourth-order accuracy even if RK4 integration were employed in the DNS.

Regardless of the accuracy of numerical methods employed, a question sometimes asked is whether numerical results are significantly affected by finite machine precision. While results given in this paper are for single precision, we have made comparisons of single and double precision for the peak dissipation and enstrophy values studied in detail in Sec. III B. For $R_\lambda \approx 390$ on a 1024^3 grid the maximum differences between peak values obtained at single versus double precision are within 0.1% and 0.16% at $C = 0.6$ and $C = 0.15$, respectively, over a time span of 10 τ_η. This percentage is likely to be higher in the case of simulations at higher grid resolution or a greater number of time steps (due to the use of smaller step size or if a longer simulation is desired). However, we have found no systematic tendency for peak dissipation or enstrophy values to be higher or lower at either level of machine precision. This indicates net effects on the results given in Sec. III below are weak, certainly much weaker than the effects of spatial and temporal resolution, provided the results are averaged over a significant period of time. This finding is also consistent with comparisons using 4096^3 and 8192^3 simulations in Ref. [1]. It is possible that machine precision has greater impact in other types of turbulent flows where fewer modes of averaging are available.

III. NUMERICAL RESULTS

Our approach in this investigation involves two key elements, both focused on the statistics of fluctuations of dissipation rate and enstrophy, which prior work has shown to possess fluctuations of extremely large magnitude. First, using the filtering operation defined earlier in Eq. (3), we assess the degree to which the far tails of the PDFs of dissipation and enstrophy may be contaminated by aliasing errors that arise when these nonlinear quantities are formed. Second, for a given Reynolds number we perform a series of short simulations where spatial and temporal resolutions are varied via $k_{\max}\eta$ and the Courant number, respectively. Simulations of large $k_{\max}\eta$ (more grid points) and low C (more time steps) are the most accurate, but also inherently expensive. However, with samples of extreme dissipation and enstrophy characterized by very short timescales, simulations of time span in the order of 10 τ_η, with statistics extracted several times per τ_η, appear to be sufficient for our purposes. At the same time, since resolution requirements for studies of small-scale intermittency are known to become more stringent at higher Reynolds numbers [7,15], it is important to perform these analyses at more than one Reynolds number. In consideration of these issues, we have performed a comprehensive series of tests at R_λ close to 390 and 650, up to 4096^3 and 8192^3 grid points respectively, as listed in Table I.

TABLE I. Resolution parameters and values of Δt as percentage of τ_η for simulation datasets at two values of the Reynolds number. Since the simulation time spans used here are short, the numbers shown are subject to statistical variability associated with the instantaneous snapshots used as initial conditions. The datasets correspond to forced simulations at R_λ of 390 and 650 in a collection of prior publications, including Ref. [15].

	$R_\lambda \approx 390$				$R_\lambda \approx 650$			
$k_{\max}\eta$	N	$C = 0.6$	$C = 0.3$	$C = 0.15$	N	$C = 0.6$	$C = 0.3$	$C = 0.15$
1.33	1024	1.31	0.699	0.349	2048	0.646	0.484	0.238
2.67	2048	0.609	0.333	0.165	4096	0.411	0.236	0.116
5.38	4096	0.327	0.164	0.082	8192	0.205	0.102	0.062

A. Filtering and resolution effects on dissipation and enstrophy

A long-standing question in intermittency theory is whether fluctuations of dissipation and enstrophy (both being measures of the small scales of turbulence) scale similarly with increasing Reynolds number [16,17]. The shapes of their PDFs are of particular interest, since they provide surrogates for "extreme events." Although their behaviors in the high Reynolds number limit are not yet established, data available so far do show that enstrophy is more intermittent than dissipation, with wider tails in the PDF. It may seem reasonable, thus, to suppose the statistics of enstrophy to be more sensitive to resolution than those of the dissipation.

Figures 1(a) and 1(b) show, in both linear-log and log-log scales, a comparison of PDFs of dissipation and enstrophy at different levels of spatial resolution, obtained by applying the filtering proposed in Sec. II. In frame (a), for both variables, the tails of the PDF become systematically narrower as the resolution is reduced. This implies contributions to the wide tails observed mostly reside in the wave numbers that are close to $k_{\max}$, which are also most prone to contamination from aliasing errors when high-order quantities are computed. The differences observed here are stronger for dissipation than for enstrophy; that is, even though less intermittent, the dissipation is more sensitive to resolution than enstrophy. If this sensitivity is different in magnitude for dissipation and enstrophy, it becomes necessary to revisit the conclusions from recent work [1,11] on whether the PDFs of the two quantities approach each other as the Reynolds number increases. In part (b) of this figure, where the x axis is extended further than in (a), a regime of power-law roll-off (linear on log-log scales) can be seen in the unfiltered results [$\epsilon/\langle\epsilon\rangle = O(1000)$ or higher]. This feature disappears when the velocity field is truncated at $k_c = 0.75k_{\max}$. An additional effect of the filtering is that at moderately intense fluctuations (say, $100 \leqslant \epsilon/\langle\epsilon\rangle < 500$) the PDF also shifts inwards when

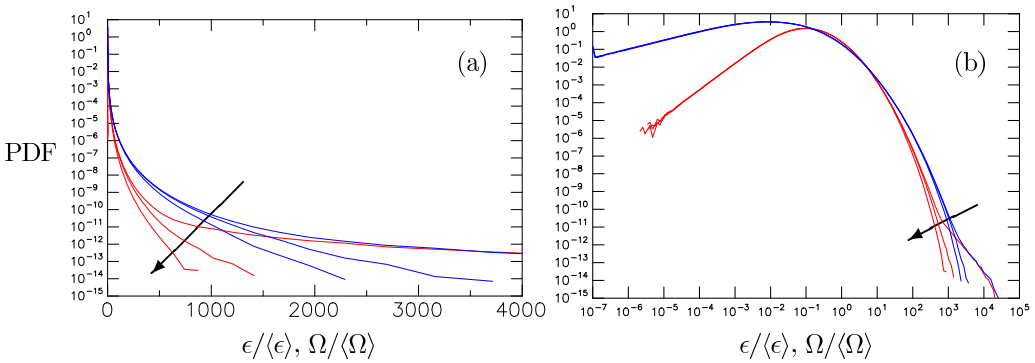

FIG. 1. PDFs of normalized dissipation rate (red) and enstrophy (blue) in (a) linear-log scales and (b) log-log scales, at $R_\lambda \approx 650, 4096^3$, $k_{\max}\eta \approx 2.8$, $C = 0.6$. Results are computed from velocity fields filtered at $k_c/k_{\max} = 1$, 0.75, and 0.5, in the direction of the arrows.

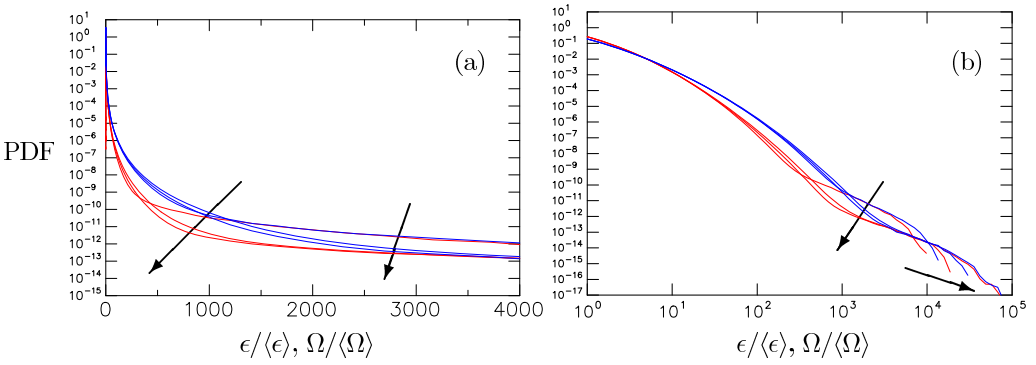

FIG. 2. PDFs of normalized dissipation rate (red) and enstrophy (blue) in (a) linear-log scales and (b) log-log scales, obtained from unfiltered velocity fields in simulations at $R_\lambda \approx 650$, $C = 0.6$. Grid resolutions 2048^3, 4096^3, and 8192^3 corresponding to $k_{\max}\eta \approx 1.4$, 2.8, and 5.6, increasing in the directions of the arrows.

more of the highest wave-number modes are removed by filtering, but this effect is more gradual with respect to changes in $k_c/k_{\max}$. Finally we also note, in frame (b), that at very small ϵ or Ω both PDFs exhibit robust power laws with positive exponents. This last feature can be explained as a consequence of velocity gradients in quiescent zones of the flow behaving as Gaussian random variables [11].

While filtering is a useful diagnostic tool as demonstrated above, obtaining accurate results requires simulations at higher resolution. In Figs. 2(a) and 2(b) we compare the PDFs in a manner similar to that in Fig. 1, using only unfiltered results at nominally the same Reynolds number but three different spatial resolutions. In frame (a) improved resolution in space is seen to reduce the likelihood of large fluctuations up to several thousands times the mean value, again with dissipation showing greater sensitivity. In frame (b) we again use log-log scales, with the scale on the x axis adjusted so that behavior at the furthest tails can be examined more clearly. As the spatial resolution is improved, the numerically spurious power-law behavior near the tails is still present, although now shifted towards even larger fluctuations. This shows, at the least, that improving spatial resolution alone does not remove all possible numerical errors.

To understand why dissipation is more sensitive to resolution, we note that, whereas both ϵ and Ω are derived from velocity gradients, longitudinal velocity gradients contribute to ϵ only. It is well known that in incompressible turbulence longitudinal velocity gradients are negatively skewed but transverse gradients, while symmetric, are more strongly non-Gaussian. In Fig. 3 we compare filtered and unfiltered results on the PDFs of longitudinal and transverse velocity gradients, as well as the PDF of a single vorticity vector component. All three variables display narrower tails when the filtering is applied, showing again that the occurrence of very large velocity gradients can be overestimated because the velocity field in the high wave-number modes are in turn contaminated by aliasing errors. It is also clear that the longitudinal gradients are more sensitive to resolution effects, while vorticity (which consists of transverse gradients alone) shows a sensitivity similar to the transverse gradients themselves.

Further insight on the contrasts between resolution effects on longitudinal and transverse velocity gradients can be had by considering one-dimensional spectra, as follows. Since incompressibility requires $\hat{\mathbf{u}} \perp \mathbf{k}$, at high $k = |\mathbf{k}|$ most of the spectral content of $\hat{u}_1$ resides in wave-number vectors orthogonal to the k_1 axis, i.e., mostly modes with small k_1 but large $k_r = \sqrt{k_2^2 + k_3^2}$ (such that k is significantly greater than k_1). Thus, for a given k_1 more energy is removed in $\hat{u}_1$ than $\hat{u}_2$ and $\hat{u}_3$ when truncation based on k is applied. This kinematic effect causes the longitudinal spectrum (of $\hat{u}_1$ in k_1) to be affected more by the truncation than the transverse spectrum (of $\hat{u}_2$ or $\hat{u}_3$ in k_1). We can also make use of the relations [18] for longitudinal and transverse energy spectra in incompressible

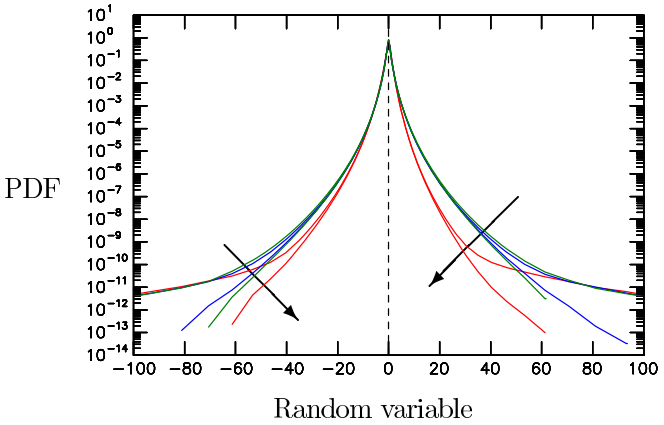

FIG. 3. Standardized PDFs of longitudinal (red) and transverse (blue) velocity gradients as well as vorticity (green), obtained from 17 snapshots in simulation with $R_\lambda \approx 650, 4096^3$, $C = 0.6$. Resolution levels $k_c/k_{\max} = 1$ and 0.5 (decreasing in the directions of the arrows).

isotropic turbulence,

$$E_{11}(k_1) = \int_{k_1}^{\infty} \frac{E(k)}{k}\left(1 - k_1^2/k^2\right)dk, \quad E_{22}(k_1) = \frac{1}{2}\int_{k_1}^{\infty} \frac{E(k)}{k}\left(1 + k_1^2/k^2\right)dk, \tag{7}$$

where $E(k)$ is the 3D energy spectrum function. If the spectrum is truncated at $k = k_c$, the longitudinal spectrum for k_1 close to k_c can be approximated as

$$E_{11}(k_1) \approx \frac{E(k_1)}{k_1}\int_{k_1}^{k_c}\left(1 - k_1^2/k^2\right)dk, \tag{8}$$

which further simplifies to $E_{11}(k_1) \approx E(k_1)(\Delta k/k_1)^2$, where $\Delta k = k_c - k_1$. Similar reasoning leads to $E_{22}(k_1) \approx E(k_1)(\Delta k/k_1)$ and hence the ratio of longitudinal to transverse spectrum at k_1 close to the cutoff becomes

$$\frac{E_{11}(k_1)}{E_{22}(k_1)} \approx \frac{\Delta k}{k_1} = \frac{k_c - k_1}{k_1} \quad (\Delta k \ll k_c). \tag{9}$$

Figure 4 shows results on $E_{11}(k_1)$, $E_{22}(k_1)$, and their ratio. The stronger sensitivity of the high wave-number region of $E_{11}(k_1)$ [compared to $E_{22}(k_1)$, in (a) of the figure] to the spectral cutoff is consistent with the finding that the statistics of longitudinal velocity gradients are more sensitive to resolution than those of the transverse gradients. In addition, in (b), for k_1 close to each choice of the cutoff k_c, the estimate (9) is seen to agree very well with actual data on the ratio $E_{11}(k_1)/E_{22}(k_1)$.

B. Tests of spatial and temporal resolution

While comparisons of results obtained before and after filtering help identify the sensitivity to resolution effects, it is still important to obtain new results at spatial and temporal resolution better than previously practiced. It would be ideal if some degree of convergence can be achieved with respect to spatial or temporal resolution if the grid spacing and time step are made increasingly smaller. To reach this objective we need to minimize a third source of uncertainty, namely that of statistical sampling. Since extreme events are of very short duration, our test simulations do not need to span a long period of time for a sufficient number of independent samples to be taken; yet sampling requirements are met by calculating dissipation and enstrophy frequently, and on the fly, at regular output steps in the DNS code. We also find it useful to follow the time evolution of simpler

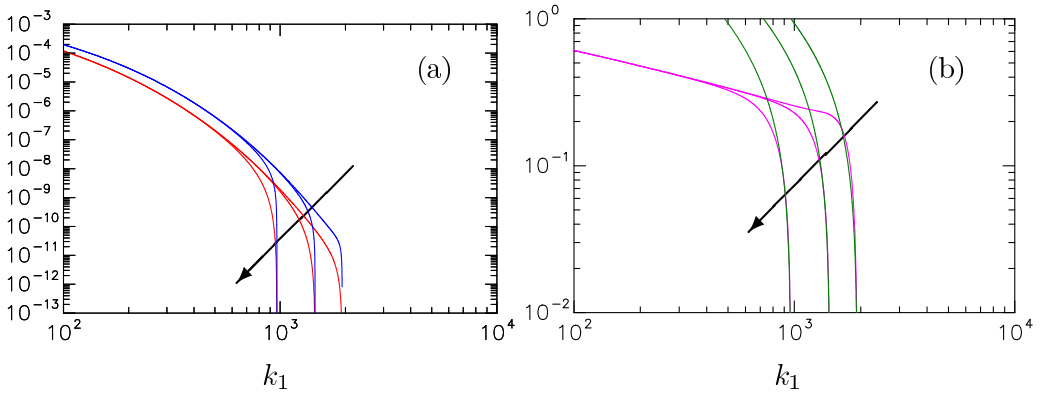

FIG. 4. (a) Longitudinal (red) and transverse (blue) 1D spectra, and (b) the ratio $E_{11}(k_1)/E_{22}(k_1)$ (magenta for actual data, green for estimate at k_1 close to k_c), with truncation levels $k_c/k_{\max} = 1$, 0.75, and 0.5 in the direction of the arrows. The plots are based on the same simulation datasets as in Figs. 1 and 2.

diagnostic quantities, namely the peak values of $\epsilon/\langle\epsilon\rangle$ and $\Omega/\langle\Omega\rangle$ taken over all grid points in the simulation.

Figure 5 shows the evolution of peak $\epsilon/\langle\epsilon\rangle$ and $\Omega/\langle\Omega\rangle$ over a period of order $10\tau_\eta$, at $R_\lambda \approx 390$, at different spatial and temporal resolutions as indicated earlier in Table I. Each frame shows the peak values (over all grid points) of $\epsilon/\langle\epsilon\rangle$ or $\Omega/\langle\Omega\rangle$ with Courant number varied for a given spatial resolution. Generally these simulations are conducted with initial conditions taken from a prior instantaneous snapshot obtained at relatively low $k_{\max}\eta$ and high C. In most cases the effects of improved resolution are quickly apparent (within 0.5 τ_η or less). It can be seen that the Courant number has a major effect: $C = 0.6$ gives considerably higher peak values of both $\epsilon/\langle\epsilon\rangle$ and $\Omega/\langle\Omega\rangle$ except

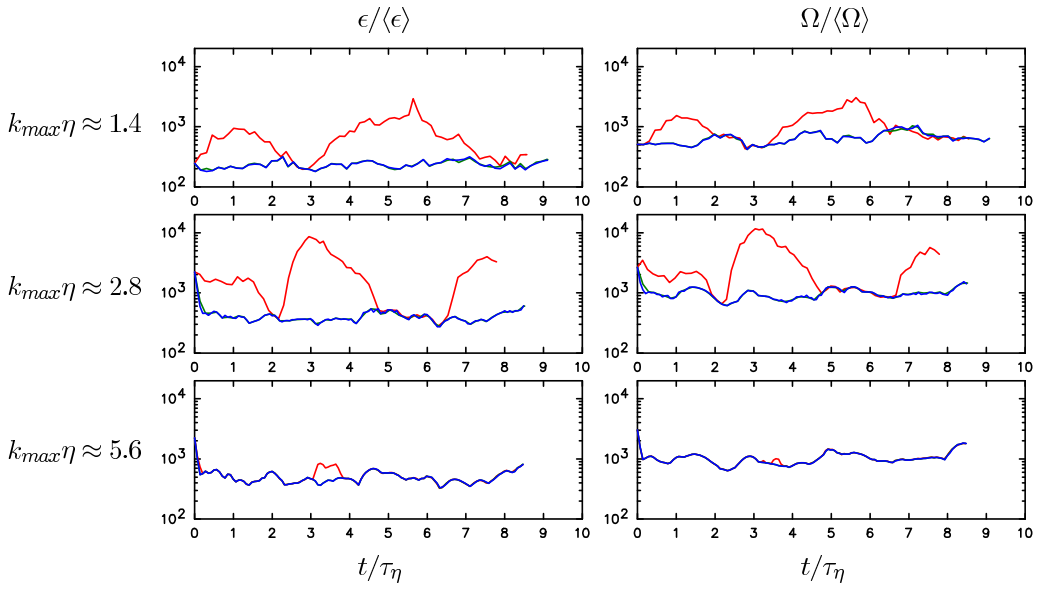

FIG. 5. Comparison of peak $\epsilon/\langle\epsilon\rangle$ (left) and $\Omega/\langle\Omega\rangle$ (right) for results obtained at different Courant numbers, $R_\lambda \approx 390$, over time spans in the order 10 τ_η. Different colors represent $C = 0.6$ (red), 0.3 (green), and 0.15 (blue). From top to bottom $k_{\max}\eta \approx 1.4$, 2.8, and 5.6 (grid resolutions 1024^3, 2048^3, 4096^3). In many places lines in green and blue are almost coincident (with only blue being directly visible).

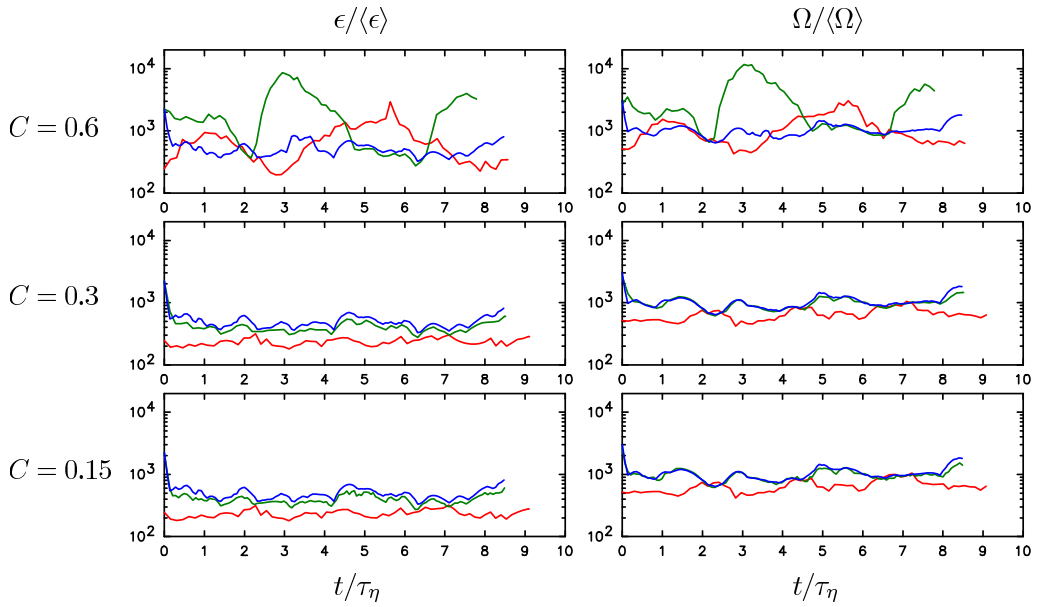

FIG. 6. Same data as Fig. 5, but with data for different $k_{\max}\eta \approx 1.4$ (red), 2.8 (green), 5.6 (blue) shown in the same frames at each given choice of the Courant number. From top to bottom: $C = 0.6$, 0.3 and 0.15.

at high spatial resolution ($k_{\max}\eta \approx 5.6$), while results for $C = 0.3$ and 0.15 agree very closely. Since there is no doubt that a lower C gives more accurate results, this comparison implies that observed peak values are overpredicted (hence spurious) in the case of $C = 0.6$. Closer observation shows the contrast between $C = 0.6$ and $C = 0.3$ is apparently greater for dissipation than enstrophy, which is consistent with results in Sec. III A that dissipation is the more sensitive quantity. At sufficiently low C the peak values are also remarkably steady in time, and somewhat higher for enstrophy than dissipation, especially at low C (e.g., the time-averaged peak values in the lowermost frames are about 480 for $\epsilon/\langle\epsilon\rangle$ and 1020 for $\Omega/\langle\Omega\rangle$, respectively). Overall it appears clear that simulation segments of $10\tau_\eta$ are sufficiently long for the present purposes.

One implication of this discussion is that attempts to produce more accurate results by improving spatial resolution may not be adequate unless one improves temporal resolution as well. To see this more clearly, in Fig. 6 we have replotted data from Fig. 5, but with each frame now holding results for a given C but for different values of $k_{\max}\eta$. If the effect of improved spatial resolution is to allow larger local gradients to be captured then the peak values should increase with $k_{\max}\eta$. This trend is supported by our results for $C = 0.3$ and 0.15. For data at these two Courant numbers, the peak values at $k_{\max}\eta = 2.8$ and 5.6 still differ more significantly in the case of the dissipation, which again suggests that dissipation is more sensitive to resolution than enstrophy.

It is now well understood, from both theory [7] and computation [15], that spatial resolution requirements for the study of intermittency become more stringent with increasing Reynolds number. A similar trend can be expected for temporal resolution Δt, which has been cast in Sec. II in terms of the advective timescale η/u' [Eq. (6)] rather than the Kolmogorov timescale τ_η [Eq. (5)]. However, neither of these estimates allows for the effects of intermittency, which may be felt via extreme velocity gradients of even smaller timescales. There is thus a possibility that, for a given $k_{\max}\eta$, the time step Δt to ensure accuracy corresponds to a Courant number that is lower than suggested by these estimates, especially as the Reynolds number increases. To answer this question we show in Fig. 7 data similar to Fig. 6, but at $R_\lambda \approx 650$. The comparison between these two figures is consistent with the expectation that extreme events intensify when the Reynolds number is increased. Differences between the results at $k_{\max}\eta$ 2.8 and 5.6 (with C fixed) become much more substantial, perhaps

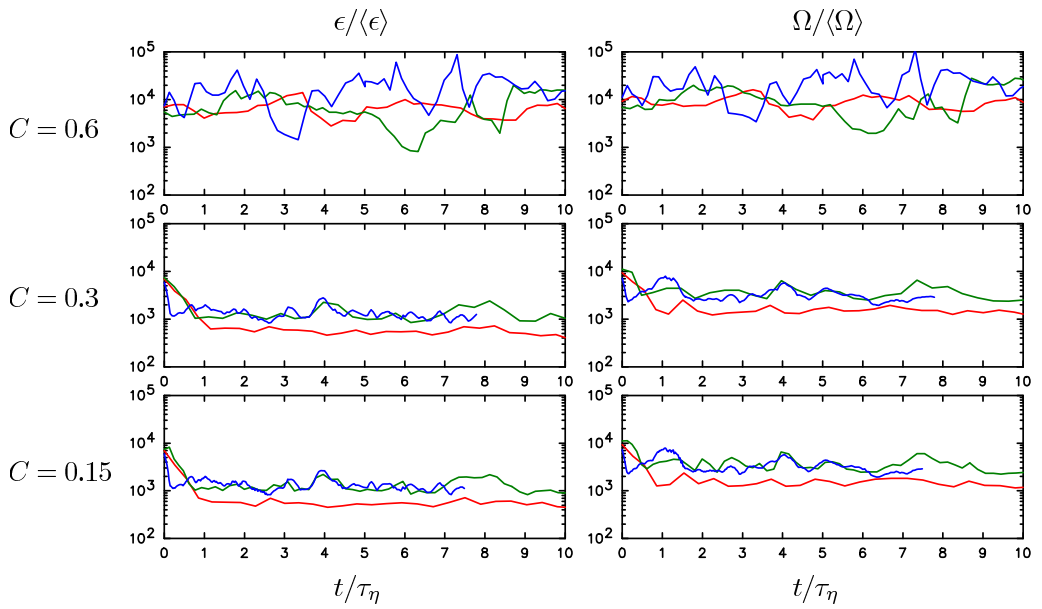

FIG. 7. Similar to Fig. 6, but at $R_\lambda \approx 650$, at grid resolutions 2048^3, 4096^3, 8192^3 for $k_{\max}\eta \approx 1.4$ (red), 2.8 (green), 5.6 (blue). From top to bottom: $C = 0.6$, 0.3 and 0.15.

somewhat erratic, even at the lowest C (0.15) that we have tested in detail. Results at $C = 0.3$ and $C = 0.15$ agree closely but not as closely as in Fig. 6. This change in level of agreement may be interpreted as indicating that, as Reynolds number increases, a lower Courant number is required to maintain a similar level of temporal accuracy.

The effects of spatial and temporal resolution on the peak values of dissipation and enstrophy, considered above, are expected to carry over directly to the behavior of the respective PDFs at extreme values of these variables. Since the peak dissipation and enstrophy signals studied above exhibit statistical stationarity in time beyond a certain initial transient, it is appropriate to take averages of the PDF results over time after excluding, say, the first 1/4 of the time period tested. In Fig. 8 we plot the PDFs at different $k_{\max}\eta$ with C fixed at 0.15. Most of the curves shown are quite smooth, suggesting adequate sampling, although of course sampling limitations are always present at extreme values where the number of samples falling into "bins" of finite size is sensitive to the statistical variability of the simulations of modest length employed in this paper. At $R_\lambda \approx 390$ (top row in this figure) results on both dissipation and enstrophy suggest that a strong degree of convergence in spatial resolution has been achieved, with the main difference between $k_{\max}\eta \approx 2.8$ and 5.6 being that the tail of the PDF stretches out wider as larger samples are captured on a finer grid. At $R_\lambda \approx 650$ (middle row in this figure) the relative positions of lines in green and blue follow the expected trend less closely than at $R_\lambda \approx 390$. To check on this feature we have verified the accuracy of the green line by comparing it with results in another simulation with C further reduced to 0.075 (and finding little significant difference). This test shows the differences between the lines in green and blue noted here are primarily statistical in nature, which can be manifested via a sensitivity to initial conditions as well as to the time spans used for averaging in the simulations. Overall it is clear that the extreme values for enstrophy are more probable than for dissipation, while both of them increase with the Reynolds number. However, sensitivity to spatial resolution is strong only for sample values beyond a certain threshold, which itself increases with the Reynolds number, and is higher for enstrophy than for dissipation.

We recall earlier in Fig. 2(b) that PDF data obtained from simulations at inadequate temporal resolution ($C = 0.6$) were characterized by an the unphysical "power-law decay" feature. The bottom

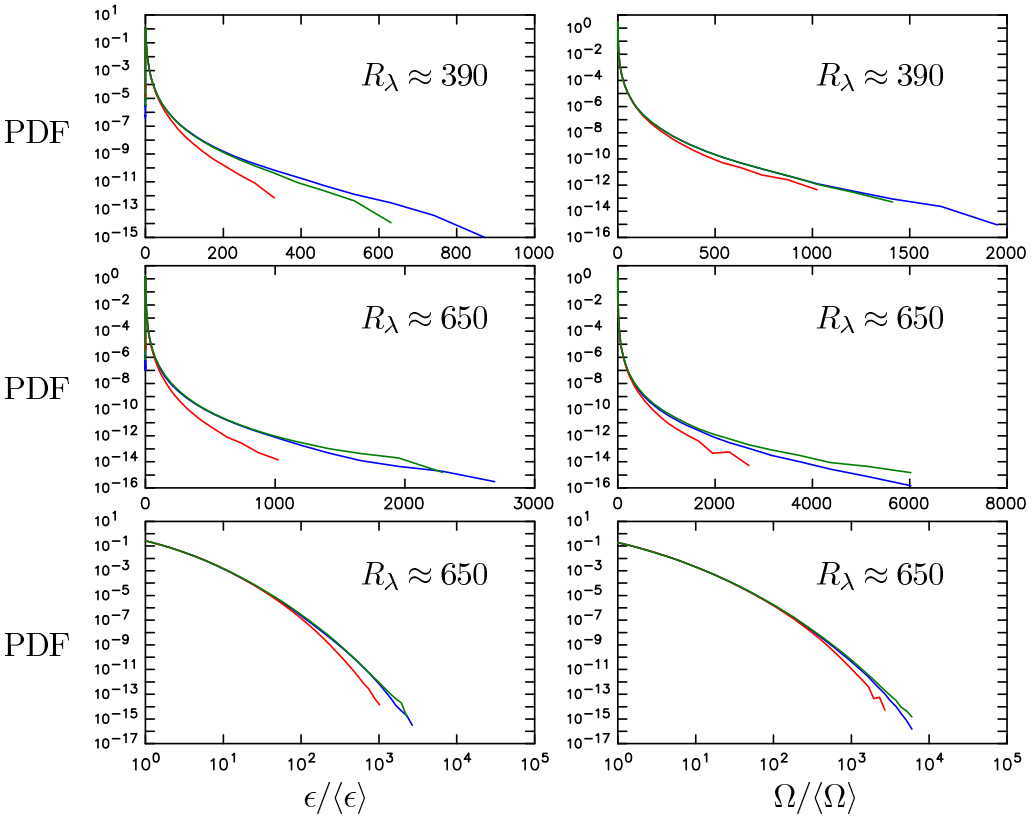

FIG. 8. PDFs of $\epsilon/\langle\epsilon\rangle$ (left) and $\Omega/\langle\Omega\rangle$ (right) for results obtained at $C = 0.15$. Top row: $R_\lambda \approx 390$; middle and bottom rows: $R_\lambda \approx 650$, on linear-log and log-log scales respectively. Different colors indicate different levels of spatial resolution: namely $k_{\max}\eta \approx 1.4$ (red), 2.8 (green), 5.6 (blue).

row of Fig. 8 shows the same data as in the middle row, but on log-log scales and in a format similar to that in Fig. 2(b). It is clear that, with improved temporal accuracy at $C = 0.15$, the unphysical result seen earlier is no longer observed.

It is understood that the sensitivity of results on extreme dissipation and enstrophy to spatial and temporal resolution is closely connected to the presence of aliasing errors, which in Rogallo [14] are not completely removed. Both dissipation and enstrophy fluctuations are obtained by differentiating in Fourier space, followed by transforming to physical space and taking the squares of strain rates and vorticity components formed in this process. Contributions from aliased modes are amplified when these squares are taken, and even more so when higher powers corresponding to higher moments are considered. However, it is possible, although expensive, to remove aliasing errors entirely from this calculation by modifying the simulation procedure such that the velocity field itself is alias-free. We consider first an N^3 grid, and truncate at half of the usual $k_{\max} = \sqrt{2}N/3$ before derivatives are formed. Equivalently, to obtain alias-free results at a resolution equivalent to an N^3 grid, we perform a simulation using $(2N)^3$ grid points but remove all spectral content (that may form as a result of nonlinearities in the Navier-Stokes equations) at $k \geqslant \sqrt{2}N/3$ (i.e., $k_{\max}$ of the N^3 grid) at every Runge-Kutta substage. The resulting numerical solution is free of aliasing errors, although truncation errors due to finite Δx and Δt remain. Figure 9 compares production DNS results at a low C with alias-free results at a higher C. The agreement is clearly excellent. In particular, since in Rogallo's scheme aliasing errors vary as $(\Delta t)^2$, aliasing errors are reduced by a factor of 16 when C is reduced from 0.6 to 0.15, thus bringing the numerical solution close to alias-free results at $C = 0.6$.

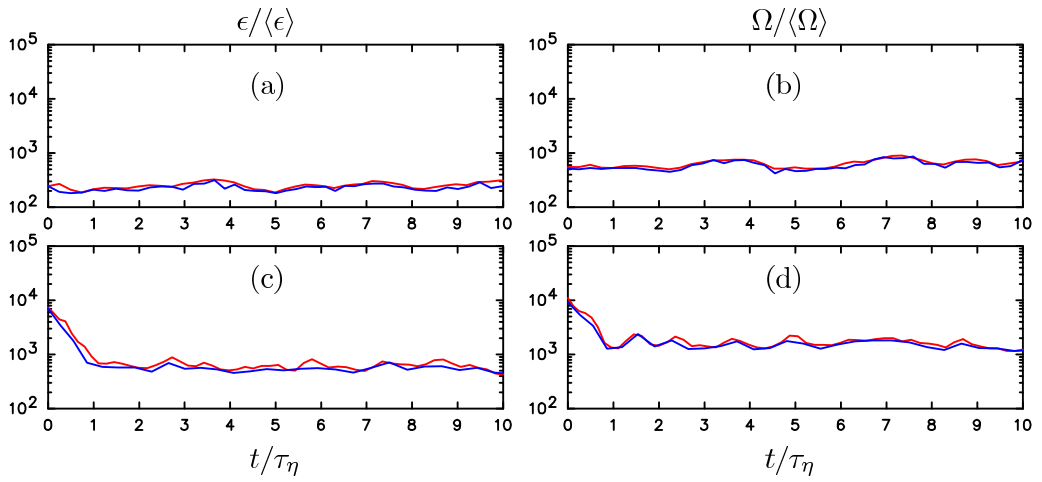

FIG. 9. Comparison of peak dissipation (left) and peak enstrophy (right), between (blue lines) DNS results at $C = 0.15$ on an N^3 grid with truncation at $\sqrt{2}N/3$ and (red lines) test results from alias-free simulation at $C = 0.6$ on a $(2N)^3$ grid also truncated at $\sqrt{2}N/3$. Frames (a) and (b): $R_\lambda \approx 390$, $N = 1024$. Frames (c) and (d): $R_\lambda \approx 650$, $N = 2048$.

Since the alias-free approach requires a $(2N)^3$ grid, at a fixed C it requires 16 times more resources (for a given physical time span) than Rogallo's scheme at $C = 0.6$, compared to four times more when C is reduced from 0.6 to 0.15 with no change in truncation in wave-number space.

C. Re-interpretation of dissipation and enstrophy PDFs at high resolution

With this improved understanding of the effects of finite resolution in both time and space, it is now useful to revisit the nature of extreme events represented by the far tails of the PDFs of dissipation and enstrophy. In particular, we are interested in the viability of stretched exponentials [19,20], and whether there is a definite trend for the tails of these two PDFs to behave similarly at high Reynolds number [1,11].

If both PDFs behave as stretched exponentials, we may write

$$f_\epsilon(\epsilon/\langle\epsilon\rangle) \sim \exp[-b_\epsilon(\epsilon/\langle\epsilon\rangle)^{\gamma_\epsilon}], \quad f_\Omega(\Omega/\langle\Omega\rangle) \sim \exp[-b_\Omega(\Omega/\langle\Omega\rangle)^{\gamma_\Omega}], \tag{10}$$

where the dependencies of the coefficients b_ϵ, γ_ϵ, b_Ω, γ_Ω on Reynolds number are of interest in intermittency scaling. Figure 10 shows the best results available for dissipation and enstrophy PDFs at two different Reynolds numbers, mostly free from shortcomings of inadequate resolution. Solid lines in red and blue represent the present DNS results, while dashed lines in the same colors represent curve fits of the forms given in Eq. (10). The current results show clearly that, as Reynolds number increases, the far tails of the PDFs remain different, and that the most extreme values of enstrophy continue to be higher than those of dissipation. This revises the conclusion of [1]. The curve fits appear to agree with the DNS data very well. The coefficients used are (i) $b_\epsilon = 6.76$, $b_\Omega = 5.47$, $c_\epsilon = \gamma_\Omega = 0.25$ at $R_\lambda \approx 390$; and (ii) $b_\epsilon = 6.25$, $b_\Omega = 5.0$, $c_\epsilon = \gamma_\Omega = 0.225$ at $R_\lambda \approx 650$. These values are chosen empirically while taking $\gamma_\epsilon = \gamma_\Omega$, based on prior work [15] and recognizing that smaller values of both the premultipliers (b_ϵ, b_Ω) and exponents $(\gamma_\epsilon, \gamma_\Omega)$ can represent PDFs of wider tails.

The fact that dissipation and enstrophy PDFs have different tails even at asymptotically high Reynolds numbers does not contradict any known result; we know only that the two quantities are equal on the mean in homogeneous turbulence. It is, however, interesting to note that the two PDFs possess a similarity in shape. For example, the tails of the PDF of $2\epsilon/\langle\epsilon\rangle$ appear to follow those of $\Omega/\langle\Omega\rangle$ quite closely, at least on the semilogarithmic scales. It is entirely plausible that better

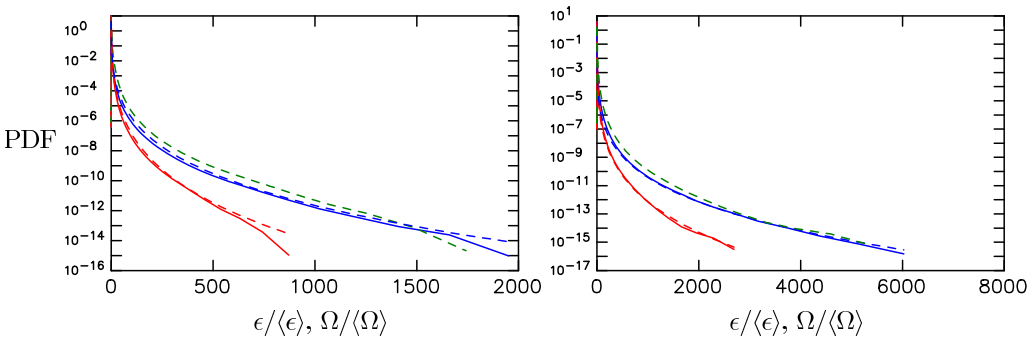

FIG. 10. PDFs of $\epsilon/\langle\epsilon\rangle$ (red) and $\Omega/\langle\Omega\rangle$ (blue) for results obtained at $C = 0.15$, $k_{\max}\eta \approx 5.6$: $R_\lambda \approx 390$ (left), $R_\lambda \approx 650$ (right). Dashed lines in green show the PDF of $2\epsilon/\langle\epsilon\rangle$. (Note the differences in range of x-axis between the two frames.)

agreement for different parts of the two tails can be had with different, amplitude-dependent scaling factors (suggesting different multifractal structures for the two quantities) but a deeper understanding of this possibility requires future work.

IV. CONCLUSIONS AND DISCUSSION

A systematic study using a combination of spectral filtering and numerical simulations at enhanced spatial and/or temporal resolution is presented, in order to clarify the proper behavior of the scaling of dissipation and enstrophy PDFs in forced incompressible isotropic turbulence. It is understood that, even in the largest simulations achievable at present, not all results are equally reliable, and accuracy in results such as high-order moments of highly intermittent quantities is inevitably more difficult to achieve. A major motivation in this paper is to reevaluate the numerical fidelity of prior results concerning the occurrence of extreme events in fluctuations of the energy dissipation rate and enstrophy, in DNS datasets with the number of grid points reaching 8192^3 and higher. While long simulations at optimal resolution and largest problem sizes are still prohibitively costly, we are able to draw useful conclusions from short simulations (per Table I) using 1024^3 to 8192^3 grid points at modestly high Taylor-microscale Reynolds numbers (390 and 650).

A procedure of removing higher wave-number modes in the velocity field via a series of sharp spectral filters is shown to lead to substantially narrower tails of the PDFs of dissipation and enstrophy, while exposing symptoms of inaccuracies (as in Figs. 1 and 2) that arise because of insufficient resolution. Although less intermittent than enstrophy (at least at the Reynolds numbers for which results are available), dissipation is more sensitive to inadequate resolution, as a result of incompressibility constraints applicable to longitudinal velocity gradients.

While concerns for limited spatial resolution (relative to the Kolmogorov length scale, η) are well known since the time it was discussed in Ref. [7], the issue of temporal resolution (beyond numerical stability) appears to have received less attention. However, our results for the far tails of the PDFs of dissipation and enstrophy, and their corresponding peak values extracted on the fly from the simulations, show strong sensitivity to temporal resolution as well, even when time step (Δt) is well under 1% of the Kolmogorov timescale. Instead, Δt must be small compared to the timescale of advective turbulent transport over one grid spacing, Δx. A sufficiently low Courant number (C), itself depending on the details of the time integration scheme, is thus necessary for the benefits of improved spatial resolution to be fully realized, for example as seen in Fig. 8 where both dissipation and enstrophy PDFs converge in the limit of high spatial resolution. Very good agreement has been demonstrated between simulation results at $C = 0.15$ with aliasing errors minimized through a small time step, by employing a more expensive approach where enforcement of a more conservative truncation criterion in wave-number space can be used to obtain alias-free results.

In summary, we have presented here a critical examination of the effects of both spatial and temporal errors on extreme events in small-scale turbulence. Full benefits of improved spatial resolution may not be attained unless temporal resolution is also adequate. We conclude that the likelihood and strength of extreme events in dissipation and enstrophy (especially the former) reported in our prior work have been, as a result of the numerical issues addressed in this paper, overestimated. With these numerical issues now clarified, we note that data in highly resolved simulations do not support a theoretical prediction that the PDFs of dissipation and enstrophy approach each other in the high Reynolds limit. However, the two PDFs are consistently similar in form.

Since the numerical errors addressed in this paper mainly affect extreme fluctuations, other past conclusions based on moderately intense fluctuations are likely to be not greatly affected. An important topic in this context is the statistics of local averages of the dissipation rate for various scale sizes. Since inertial range motions at high Reynolds numbers are large compared to the grid spacing, they are less sensitive to resolution effects than results in the dissipation range where the most intense fluctuations occur. A subsequent paper will be devoted to the study of such local averages using DNS datasets with up to $16\,384^3$ grid points.

ACKNOWLEDGMENTS

This work is supported by the National Science Foundation via Grants No. 1036180 and No. 1640771 under the Petascale Resource Allocations Program of the Office of Advanced Cyberinfrastructure. The first author is particularly grateful for great assistance received from consultants and staff members on the Blue Waters Project, which is supported by NSF at the National Center for Supercomputing Applications, University of Illinois at Urbana-Champaign. In addition, a substantial number of the simulations reported in this paper were performed on the Stampede2 supercomputer at the Texas Advanced Computation Center of the University of Texas at Austin, under an Early User program for new Skylake nodes of Phase 2 of the system in late 2017. We thank D. Buaria, A. Pumir, J. Schumacher, and V. Yakhot for helpful discussions. Valuable comments from referees that have helped us improve this paper are also much appreciated.

[1] P. K. Yeung, X. M. Zhai, and K. R. Sreenivasan, Extreme events in computational turbulence, Proc. Nat. Acad. Sci. USA **112**, 12633 (2015).

[2] T. Ishihara, K. Morishita, M. Yokokawa, A. Uno, and Y. Kaneda, Energy spectrum in high-resolution direct numerical simulation of turbulence, Phys. Rev. Fluids **1**, 082403 (2016).

[3] M. Lee and R. D. Moser, Direct numerical simulation of turbulent channel flow up to $Re_\tau \approx 5200$, J. Fluid Mech. **774**, 395 (2015).

[4] T. Watanabe, J. J. Riley, S. M. de Bruyn Kops, P. J. Diamessis, and Q. Zhou, Turbulent/non-turbulent interfaces in wakes in stably stratified fluids, J. Fluid Mech. **797**, R1 (2016).

[5] P. K. Yeung, S. B. Pope, A. G. Lamorgese, and D. A. Donzis, Acceleration and dissipation statistics of numerically simulated isotropic turbulence, Phys. Fluids **18**, 065103 (2006).

[6] T. Ishihara, Y. Kaneda, M. Yokokawa, K. Itakura, and A. Uno, Small-scale statistics in high resolution direct numerical simulation of turbulence: Reynolds number dependence of one-point velocity gradient statistics, J. Fluid Mech. **592**, 335 (2007).

[7] V. Yakhot and K. R. Sreenivasan, Anomalous scaling of structure functions and dynamic constraints on turbulence simulations, J. Stat. Phys. **121**, 823 (2005).

[8] J. Schumacher, K. R. Sreenivasan, and P. K. Yeung, Very fine structures in scalar mixing, J. Fluid Mech. **531**, 113 (2005).

[9] H. Tennekes, Eulerian and Lagrangian microscales in isotropic turbulence, J. Fluid Mech. **67**, 561 (1975).

[10] K. R. Sreenivasan and R. A. Antonia, The phenomenology of small-scale turbulence, Annu. Rev. Fluid Mech. **29**, 435 (1997).

[11] P. K. Yeung, D. A. Donzis, and K. R. Sreenivasan, Dissipation, enstrophy and pressure statistics in turbulence simulations at high Reynolds numbers, J. Fluid Mech. **700**, 5 (2012).
[12] D. A. Donzis and P. K. Yeung, Resolution effects and scaling in numerical simulations of passive scalar mixing in turbulence, Physica D **239**, 1278 (2010).
[13] V. Eswaran and S. B. Pope, An examination of forcing in direct numerical simulations of turbulence, Comput. Fluids **16**, 257 (1988).
[14] R. S. Rogallo, Numerical experiments in homogeneous turbulence, NASA Technical Memorandum 81315, NASA Ames Research Center, 1981.
[15] D. A. Donzis, P. K. Yeung, and K. R. Sreenivasan, Dissipation and enstrophy in isotropic turbulence: scaling and resolution effects in direct numerical simulations, Phys. Fluids **20**, 045108 (2008).
[16] S. Chen, K. R. Sreenivasan, and M. Nelkin, Inertial Range Scalings of Dissipation and Enstrophy in Isotropic Turbulence, Phys. Rev. Lett. **79**, 1253 (1997).
[17] M. Nelkin, Enstrophy and dissipation must have the same scaling exponents in the high Reynolds number limit of fluid turbulence, Phys. Fluids **11**, 2202 (1999).
[18] S. B. Pope, *Turbulent Flows* (Cambridge University Press, Cambridge, 2000).
[19] U. Frisch, *Turbulence: The Legacy of A. N. Kolmogorov* (Cambridge University Press, Cambridge, 1995).
[20] J.-R. Luévano, Statistical features of the stretched exponentials densities, J. Phys.: Conf. Ser. **475**, UNSP 012008 (2013).